Experimental and computational investigation of the effect of blade sweep on acoustic characteristics of axial fan

Minjun Park[a], Duck-Joo Lee[a], Hakjin Lee[b*]

[a] Department of Aerospace Engineering, Korea Advanced Institute of Science and Technology (KAIST), Daejeon, 34141, South Korea

[b] School of Mechanical and Aerospace Engineering, Gyeongsang National University, Jinju, Gyeongnam, 52828, South Korea

*Corresponding author e-mail address: hlee@gnu.ac.kr

Abstract

The swept blade is one of the most efficient and practical techniques to alleviate the noise radiated from rotating fans. In this study, the swept effects of an automotive cooling fan on its acoustic characteristics were investigated using numerical and experimental approaches. Straight, forward, and backward-swept blades with a serrated shroud configuration were fabricated for the automotive cooling systems, and their performance and noise levels were measured. Moreover, measurements on the acoustic spectra were used to validate the numerical predictions. The pressure fluctuation on the cooling fan system, including the fan and shroud, was calculated from unsteady computational fluid dynamics simulation, and the acoustic signal at observer positions was predicted using an acoustic analogy. The swept effects in terms of noise reduction were compared for all three swept blades. Results indicate that the sweep angle in the forward direction can reduce the noise level of the cooling fan with a serrated shroud. Hence, the characteristics of the noise source caused by swept blades surrounding the shroud were identified in automotive cooling fans. Our findings in the present study provided significant insight into the acoustic characteristics depending on the direction of the swept blade, they can be used as a guide for designing a low-noise fan blade.

Keywords: Axial fan, Sweep effect, Noise measurement, Computational Fluid Dynamics (CFD), Acoustic analogy

1. Introduction

Most automobiles with an internal combustion engine are equipped with a cooling fan placed between the radiator and the engine, and this cooling system is the primary cooling source in an automotive engine. Rotating fan blades pull the external air through the radiator, and cooling air helps maintain the coolant temperature within a stable range. Driving an automobile with a failed cooling system could lead to engine overheating. Therefore, the cooling fan is a crucial component in an automotive engine cooling system. However, the fan's noise is one of the principal noise sources in automobiles. The noise generated by the rotating fan blades could exceed permitted levels of noise pollution. This causes inconvenience to drivers or passengers in the car as the cooling fan system is designed to operate normally when the automobile is stationary or moving at low speeds. Therefore, many researchers have attempted to mitigate pollution due to noise from cooling fans by developing innovative technologies or optimization of the design of the fan blade [1-5].

The sweep and dihedral angles have been widely used as the design parameters, which define the planform geometry of the blades to design high-efficiency and low-noise fan blades,. The swept blade has either a backward or forward angle between a hub-tip line of the blade and the rotating center-hub line. Meanwhile, the dihedral (or anhedral) angle is the upward (or downward) angle from the horizontal axis of the rotor blade. We focused on the swept effect in terms of noise reduction, and then we investigated the acoustic characteristics of the swept cooling fan using experimental and numerical approaches. The concept of sweep angle is from a jet aircraft for delaying the shock waves, leading to decreasing aerodynamic drag force caused by the compressibility effect. Smith and Yeh [6] presented a blade design method including sweep effects. Using computational methods, Denton *et al*. [7] investigated the effects of the blade sweep on the aerodynamic performance and shock pattern that occur around transonic fans. They found that the forward sweep produces a better stall margin and maintains high efficiency over a wider range. Cummings [8], Fukuno [9], and Fujita [10] experimentally demonstrated that applying reasonable amounts of sweep angle could be an efficient technique in reducing fan noise depending on the inflow environment. Kerschen [11] and Envia [12] introduced a theoretical basis for selecting a distribution of sweep angles on the blades. They showed that the sweep angles could reduce an interaction noise associated with turbulence ingestion. Hanson [13] theoretically investigated the benefit of swept blades based on the interaction between geometrical shape and harmonic noise radiation in terms of acoustics. In particular, noise reduction mechanisms for swept blades have been analyzed in various fields [14-17]. Bamberger and Caroluset [18] designed an optimal low-pressure axial fan that can maximize efficiency and minimize sound emission by modifying the sweep strategy. Hurault *et al*. [19] conducted an experimental and numerical study of the sweep effect on three-dimensional flow downstream of axial flow fans. Zenger *et al*. [20] experimentally investigated acoustic characterization of forward and backward-swept fans based on inflow turbulence intensity. Herold et al. [21] identified the sound source on three different axial fans with unskewed, backward-, and forward-skewed blades through noise measurements using a standardized fan test chamber and microphone arrays. They also discussed in detail the influence of blade design on the radiated noise.

Many studies [22-26] have focused mainly on the cooling fan system without a shroud configuration. In a previous study, we identified the primary sources of broadband noise generated by a shrouded automotive cooling fan system through noise measurements and a hybrid approach, unsteady Reynolds-averaged Navier–Stokes (RANS) simulation, and acoustic analogy based on the Ffowcs Williams-Hawkings (FW-H) equation. This study is a follow-up to previous research [27]. The current study mainly aims to investigate the effects of sweep direction on the noise level and flow physics occurring around the automotive cooling fan system comprising seven blades and a serrated shroud. Further, three types of blades with different radial sweep angles were fabricated in an automotive cooling fan module, and their noises were measured in a semi-anechoic chamber. The experimental data were used to validate numerical predictions. Both measurements and numerical results were investigated to analyze the acoustic characteristics of the automotive cooling fan system, including the shroud. The noise level of the straight, forward- and backward-swept blades were examined, and the sweep effect in terms of noise reduction was discussed in detail.

2. Experimental setup and numerical method

2.1 Geometry of swept fan

In this section, we define the geometries of straight, backward, and forward-swept fans. An automotive cooling fan comprises a hub with a diameter of 154 mm, seven blades, and a band with a diameter of 390 mm that connects the blades. The blade planform was designed using Hanon systems in terms of chord and twist distribution and the shape of the sectional airfoil, and additional information about the geometry of swept fans from a previous paper was included [27]. The straight and swept blades were designed to examine the noise characteristics of the fans depending on the sweep direction. Fig. 1(a) presents the definition of the sweep angle. The straight fan shows that the hub-tip line of the blade has no sweep angle, as illustrated in Fig. 1 (b). The rotational direction of the fan is counter-clockwise when viewed from the front. The forward-swept blade is the fan configuration wherein the hub-tip line of the blade has a forward sweep along the direction of rotation. However, the hub-tip line of the backward-swept blade has a backward sweep along the counter-direction of the rotation, as presented in Figs. 1 (c) and (d).

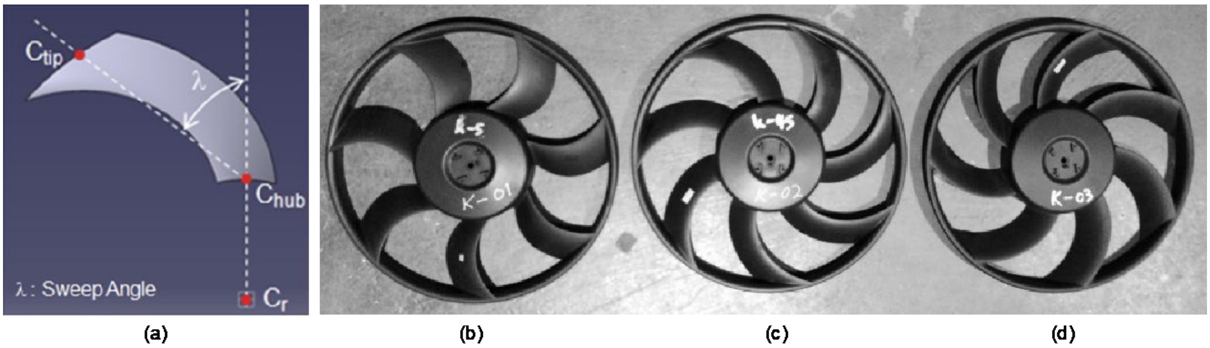

Fig. 1. Geometries of automotive cooling fan: (a) definition of sweep angle of fan, (b) straight fan with no sweep angle, (c) swept fan with 45° forward sweep angle, and (d) swept fan with 45° backward sweep angle

2.2 Noise measurement of an automotive cooling fan system

The radiated noise of the three types of fans comprising straight, forward, and backward-swept blades was measured under the free-field condition in a semi-anechoic chamber where sound reflections do not occur. An anechoic chamber is designed to minimize sound reflections as well as external noise. It is built surrounding the test section with absorption materials and a thick concrete wall, which help to provide the non-reflecting condition and attenuate the sound pressure transmitted through chamber. The anechoic chamber used in the study has a size of 6 × 5 × 4 m (H) and sound-absorbing wedges, which achieve a cut-off frequency of 180 Hz. For the measurement, a test jig was fabricated to ensure that the center of the shrouded fan was set 0.65 m from the ground to minimize the influence of the ground. A microphone was installed in front of the center of the fan hub toward the inflow direction with a distance of 1 m in accordance with ISO 1680, as illustrated in Fig. 2 (a). Fig. 2 (b) shows the measuring equipment and experimental apparatus. The rotational speed of the fan was measured through the tachometer, and it was controlled by the current and voltage of the DC power supply. A half-inch type 4190 Bruel and Kjaer (B&K) microphone was used to measure the sound pressure level of the testing fans. It has a nominal sensitivity of 50 mV Pa^{-1} and a flat frequency response of up to 20 kHz, and it was connected directly to the B&K Nexus 2690 amplifier. Before data acquisition, the magnitude sensitivity of the microphone was adjusted using the B&K model 4231 sound calibrator. The sound calibrator provided a continuous and known sound pressure level when it was fitted on sound measuring equipment. Sound pressure measured by the microphone was collected using a National Instruments (NI) PXI-4462 24-bit digitizer. To obtain the acoustic data more periodically, we acquired and calculated the time-averaged sound pressure level ($L_{p,t}$) for 10 s by using LabVIEW in accordance with ISO 3740. The 10 times the logarithm to the base 10 of the ratio of the time average of the square of the sound pressure (P) during a stated time interval of duration (T) (starting from t_1 and ending to t_2), to the square of a reference value, $P_{ref} = 20\mu\text{Pa}$, was expressed in decibels as follows:

$$L_{p,t} = 10\log\left[\frac{\frac{1}{T}\int_{t_1}^{t_2} p^2(t)dt}{p_{ref}}\right] \qquad \text{Eq. (1)}$$

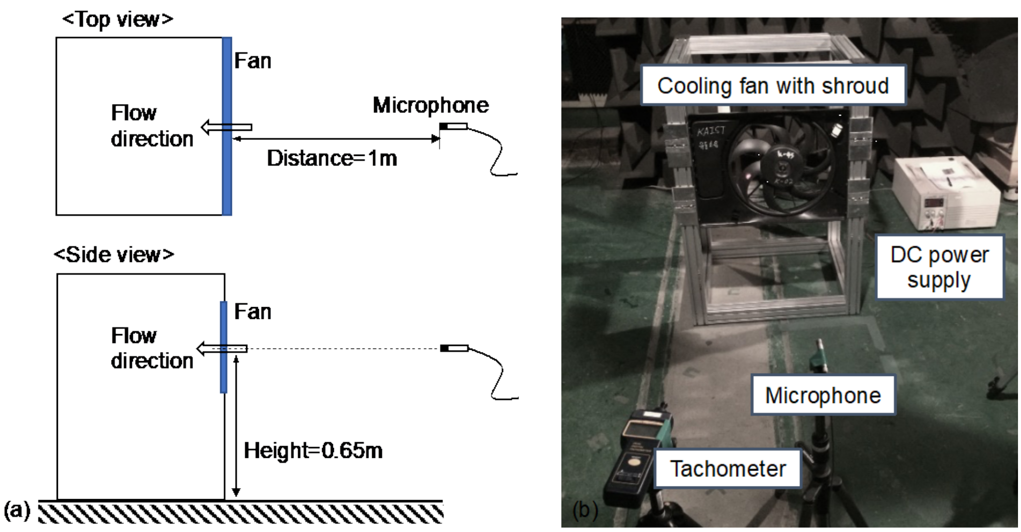

Fig. 2. Experimental setup: (a) location of a microphone and (b) measuring equipment in the semi-anechoic chamber [27]

2.3 Hybrid method for fan noise prediction

In this study, a hybrid method that used an acoustic analogy based on the FW-H equation with the noise sources evaluated from an unsteady RANS simulation was used to assess the noise level radiated from the automotive cooling fans. The essential parts of CFD simulation and acoustic analogy are presented in this paper to ensure brevity. An unsteady flow through the cooling fan was simulated using the CFD software of ANSYS CFX 14.0. Incompressible RANS equations were discretized using a cell-centered finite volume method, and the discretized equations were solved using a bounded second-order advection method with the monotonic upstream-centered scheme for conservation laws scheme for highly accurate numerical solutions. The $k - \omega$ shear stress transport (SST) turbulence model [28] with scalable wall function was used for capturing the turbulent flow. The turbulent velocity fluctuation is 5% of freestream inflow, and the turbulence length scale is 20 mm based on the fan's diameter. An implicit time integration scheme based on the second-order backward Euler equation was applied to obtain time-accurate solutions. The numerical analysis for steady-state was simulated initially until it converged, and then the unsteady analysis was performed continuously to reduce calculation time. After convergence for unsteady calculation, the results for the last three revolutions were used for acoustic prediction. The azimuth step for the unsteady fan simulation is one degree per time step, and it corresponds to a time step of 9.26×10^{-5} s.

In this study, flow through the cooling fan is considered incompressible since the tip Mach number is 0.11 at a nominal operating condition, where the rotational speed of the fan is 1,800 rpm. At the nominal operating condition, the blade tip velocity is 36.8 m/s, and the Reynolds number is 4.8×10^5. The computational domain for the CFD simulation was modeled as a rectangular box of dimensions 15 $D \times 10\ D \times 10\ D$, where D is the fan diameter. This domain includes the stationary domain for capturing high-resolution fan wake, as presented in Fig. 3 (a), and the rotating domain for applying a sliding mesh technique, as displayed in Figs. 3(b) and (c). The axial fan was surrounded by the rotating domain, which was located at 3D upstream, and 5D downstream of the fan, and the number of mesh for the rotating domain was obtained from the grid refinement study in terms of the fan performance. Note that the inner part of the shroud has serrated shapes near the rotating fan tip and the band, as depicted in Fig. 3(d). The grid resolution at the tip gap between the blade tip and shroud is one of the important factors in determining the accuracy of flow simulation since the tip leakage flow occurs at the tip gap region [29]. This leakage flow induces the strong flow interaction and disturbs the developing helical wake structure, thus leading to an increase of vortex instability and fast breakdown of wake structure. The tip leakage flow has a significant influence on the performance and noise level of the axial fan system. The grid refinement test was conducted to define the number of boundary layers in a narrow space of approximately 3 mm clearance between the fan blade and the shroud in the previous study [27]. The intermediate grid with six prism layers was used. The unstructured hybrid mesh consisting of hexahedral, prismatic, and tetrahedral elements was employed for the remaining fan blade and shroud. The total numbers of node and element were about 5.2 million and 18.3 million, respectively. The opening boundary condition was imposed on the boundary of the far-field domain, and no-slip boundary condition was applied at the surfaces of the cooling fan system, including the fan blades and shroud.

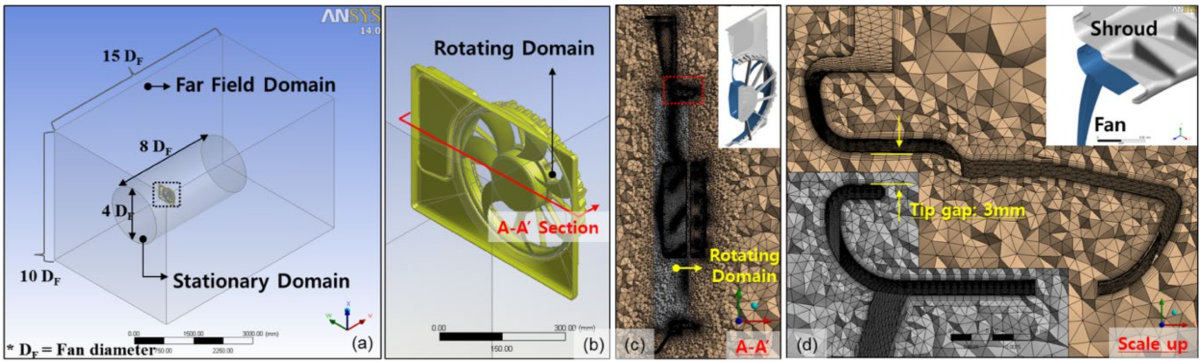

Fig. 3. Computational domain and mesh: (a) the size of computational domain, (b) rotating domain, (c) sectional view of rotating domain mesh, and (d) scale-up in the vicinity of the gap between the blade tip and the shroud [27]

In this study, the FW-H equation based on Lighthill's acoustic analogy [30] is employed to predict the sound pressure level radiated from the automotive cooling fan system comprising rotating blades and serrated shroud. Thus, the FW-H equation [31] can be expressed as

$$\left(\frac{\partial^2}{c_0^2\partial t^2}-\nabla^2\right)p'(x,t)=\frac{\partial}{\partial t}\left\{\left[\rho_0 v_n+\rho(u_n-v_v)\right]\delta(f)\right\} \\ -\frac{\partial}{\partial x_i}\left\{\left[\Delta p_{ij}n_j+\rho u_i(u_n-v_v)\right]\delta(f)\right\}+\frac{\bar{\partial}^2}{\partial x_i\partial x_j}\left[T_{ij}H(f)\right] \qquad \text{Eq. (2)}$$

Here, p is static pressure at the sources, p' is acoustic pressure at the observer, ρ is the air density, c_0 is the speed of sound, u_i is flow velocity, u_n is normal surface velocity, and n_j is the surface normal vector. Further, $\delta(f)$ and $H(f)$ are Dirac-delta and Heaviside functions, respectively, and T_{ij} is Lighthill's stress tensor for acoustic field and can be expressed as follows:

$$T_{ij}=\rho u_i u_j+p_{ij}-c_0^2\rho\delta_{ij} \qquad \text{Eq. (3)}$$

The three source terms on the right-hand side of Eq. (2) are called the monopole, dipole, and quadrupole sources, respectively. Neise reported that the dipole sources are dominant in the fan noise by the unsteady force fluctuation at low Mach number [32]. Moreover, several researchers used the dipole term to predict the surface force fluctuation of blades and propellers [33, 34, 35]. Therefore, in this study, the sound field generated by the unsteady perturbation forces of blades was considered using the dipole term of acoustic analogy. The dipole source term can be calculated using Lowson's formula that is used for moving point sources for distributed loading forces. This formula can be expressed as follows:

$$4\pi r p'(x,t) = \sum \left[\frac{1}{c_0(1-M_r)^2} \left(\dot{F}_r + \frac{F_r \dot{M}_r}{(1-M_r)} \right) + \frac{1}{r(1-M_r)^2} \left(F_r \frac{(1-M^2)}{(1-M_r)} + F_i M_i \right) \right]_{ret} \qquad \text{Eq. (4)}$$

Here, r is the distance between the observer (x_i) and source (y_i), M_i is Mach number of the source, and F_i is the force at the source. In addition, M_r and F_r are Mach number for the source and force of the source in a radiation direction, respectively. The square brackets [ ] denote the evaluation of their contents at retarded time (=source time, τ). Two measures of time should be considered when addressing acoustics problems: the retarded time when a sound signal is emitted by a source and the observer time (t) when the signal reaches at the observer. The observer time and the retarded time are expressed by the following equation:

$$t = \tau + \frac{r}{c_0} \qquad \text{Eq. (5)}$$

The source-time-dominant algorithm has been used to efficiently calculate observer times from retarded time of each moving source. Further, the acoustic pressure signal at the observer is calculated by the superposition of radiated acoustic signal from several point sources on the digitized surface of the structures. The sixth-order time derivatives obtained from the source signal were applied. Only time-series data after three revolutions, rather than the overall time history across all revolutions, were utilized on the obtained acoustic results in the frequency domain.

3. Results and discussion

3.1 Performance and noise measurements

The axial cooling fan operates under various system resistance conditions, which are key parameters that define the performance and noise level of the fan. The system resistance is the static pressure, which is the pressure difference between the inlet and outlet of the cooling fan. The inlet pressure is considered as the pressure at the position in front of the fan, while the outlet pressure is measured behind the fan. The system resistance determines the volume flow rate of air passing through the fan. If the fan operates under the system resistance of zero, called a free-field condition, the fan can deliver the maximum volume of air without any resistance. In the study, the two metrics of fan performance and noise were used to validate the numerical prediction results. Table 1 presents the comparison of experimental and numerical results for the mass flow rate passing through the straight, forward, and backward-swept fans. As also shown in the table, the rotational speed of each fan at zero system resistance is slightly different within the range of approximately 60 rpm, and the mass flow rate is slightly different depending on the sweep directions. It is observed that the mass flow rates computed through the CFD simulation are well-matched with the measurements within a margin of 4%, particularly in terms of both its magnitude and variations depending on the sweep directions. Both measurements and numerical simulations indicate that the straight and backward-swept fans have nearly the same mass flow rate, but the forward-swept fan has a lower mass flow rate than the others.

Table 1. Comparison of the experimental and numerical results for the mass flow rate

Conditions		Measurements	Numerical prediction	Error (%)
Fan type	RPM	Mass flow (kg/s)	Mass flow (kg/s)	
Straight fan	1807	1.07	1.09	1.87%
Forward-swept fan	1830	1.01	0.97	3.96%
Backward-swept fan	1865	1.09	1.11	1.83%

Table 2. Comparison of experimental and numerical results for OASPL

Conditions		Measurements	Numerical prediction	Error (dBA)
Fan type	RPM	OASPL (dBA)	OASPL (dBA)	
Straight fan	1807	73.7	74.4	0.7
Forward-swept fan	1830	69.8	69.2	0.6
Backward-swept fan	1865	73.5	73.1	0.4

Noise measurements on the straight and swept fans under the free-field condition in the semi-anechoic chamber were conducted to validate the numerical predictions. The overall sound pressure levels (OASPL) of the three types of fans obtained through experiments and numerical simulations are listed in Table 2. Here, the unit of dBA indicates an A-weighted sound pressure level. The measured OASPL of the straight, forward, and backward-swept fans are 73.7, 69.8, and 73.5 dBA, respectively, at each corresponding rotational speed when the system resistance is zero, while their OASPL levels predicted by the hybrid method are 74.4, 69.2, and 73.1 dBA at the same rotational speeds as in the experiments. Further, the discrepancies in the magnitude of OASPL between the experiments and numerical predictions were less than approximately 1 dBA, as listed in Table 2. The variations in the magnitude of measured OASPL depending on the sweep direction also appear to be similar to those of the predicted OASPL, as shown above in the mass flow rates.

Figure 4 shows the comparison of the predicted and measured sound spectra at the observer position for the straight, forward, and backward-swept fans, respectively. The frequency resolution of the measured fan noise is 1 Hz, while that of the predicted fan noise is 10 Hz, which is calculated at 0.1 s on the CFD analysis (three-revolution data). The tonal noises associated with the blade passing frequency (BPF) and its harmonics were observed at principal blade-associated frequencies between 210 Hz and 1,087 Hz, and the most dominant tonal noise occurred at the second BPF. The tonal noise generated by the passage of air over the blade is a dominant component in determining the overall noise level of the fan. The numerical results obtained by acoustic analogy were accurately predicted within approximately 3 dB compared to the experimental data for the three different fan blades. However, the numerical predictions tended to underestimate the higher harmonic BPFs and broadband noises, even though the tonal acoustic amplitudes at the dominant harmonics corresponding to the first, second, and third BPFs, were in good agreement with the measurements. Moreover, the tonal noise caused by the electric motor occurred at frequencies between 1.2 kHz and 2.2 kHz. However, the prediction model for motor noise was not included in this study. It is observed that the high-frequency sound pressure levels above 4,000 Hz tended to decay with frequency due to the numerical dissipation error. This indicates that the noise sources formed by the unsteady wake interaction between rotating fans and the near geometric components, such as the fan band or the serrated shroud, are well-predicted [27]. The results indicate the hybrid method used in this study can predict the acoustic characteristics of the automotive cooling fan with the shroud configuration. The numerical simulation data were used to identify the primary noise sources of the straight and swept fans. Further, these data were analyzed to investigate the effects of the sweep directions on the acoustic characteristics of fans. The sweep effects and flow physics that occur around the automotive cooling fan system with the shroud are discussed in detail in the following section.

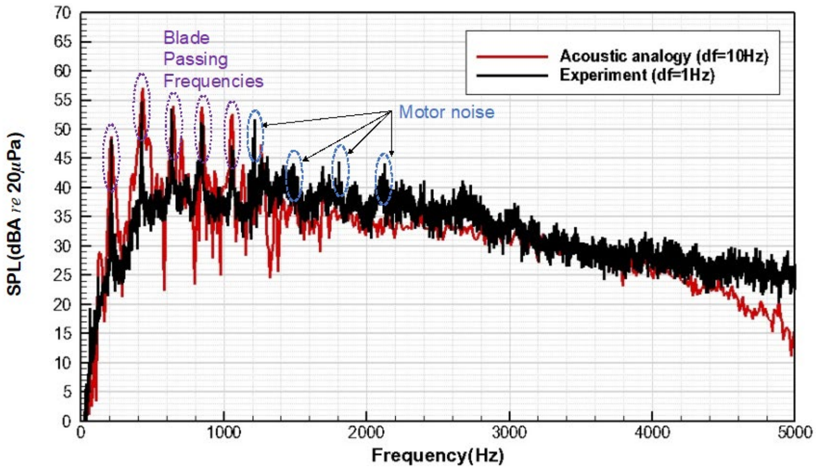

(a) Straight fan

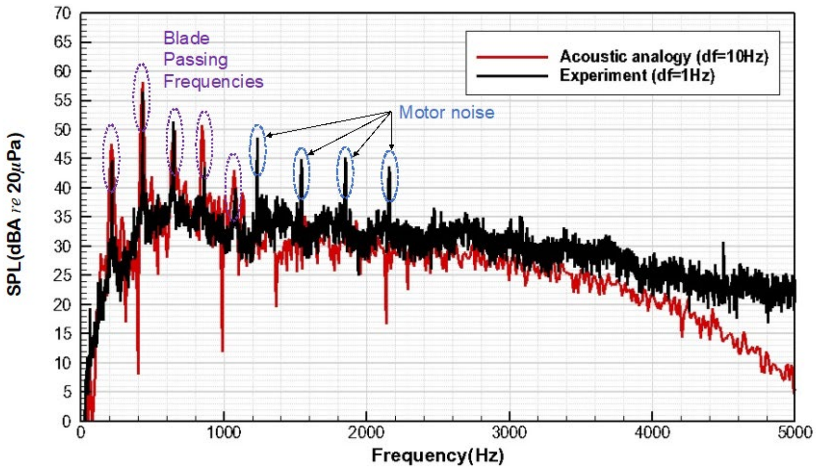

(b) Forward-swept fan

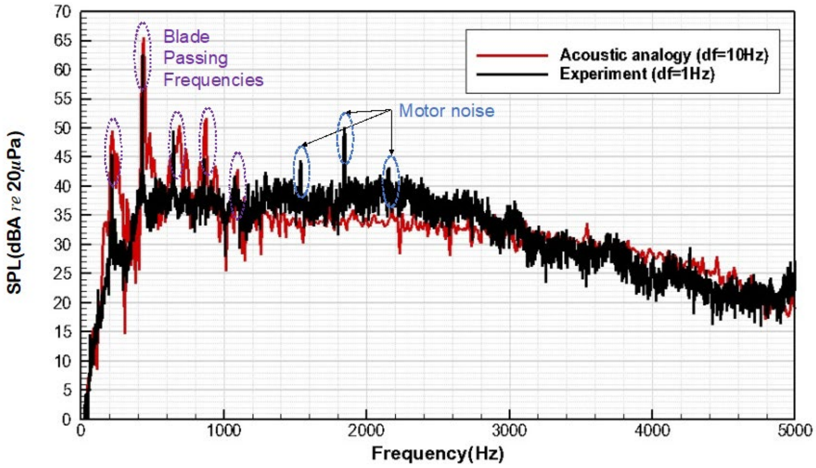

(c) Backward-swept fan

Fig. 4. Comparison of the calculated and measured noise spectra

3.2 Sweep effects

In this study, the main goal is to examine the sweep effects on the sound pressure level of an automotive cooling fan. Fig. 5 presents the overall A-weighted sound pressure levels of the straight, forward- and backward-swept fans depending on rotational speeds. The measurements are marked with the filled symbols, whereas the numerical predictions are marked with the open symbols. Note that the most considerable reduction in the overall A-weighted sound pressure level was achieved in the forward-swept fan. It is also observed that the OASPL of the straight fan is about 5 dBA higher than that of the forward-swept fan at the same rotational speed. In addition, the OASPL of the straight fan at the rotational speed of 1,600 rpm appears to be similar to that of the forward-swept fan at the rotational speed of 1,900 rpm. The experimental results indicated that a reduction of about 1 dBA was also successfully achieved in the backward-swept fan at the same rotational speed compared to the straight fan. Further, the OASPL of the forward-swept fan is about 4 dBA quieter than that of the backward-swept fan. The noise measurements demonstrate that, for a wide range of rotational speeds, sweep effects effectively decrease the OASPL of the automotive cooling fans. The previous researchers theoretically presented that it changed the phase of the peak noise because the peak noises were dispersed by swept blades [8]. However, at the same rotational speed, the noise difference between the backward-swept fan and the forward-swept fan is still approximately 4 dBA. Therefore, the noise and performance of the fan surrounding the serrated shroud became different depending on the direction of the blade sweep.

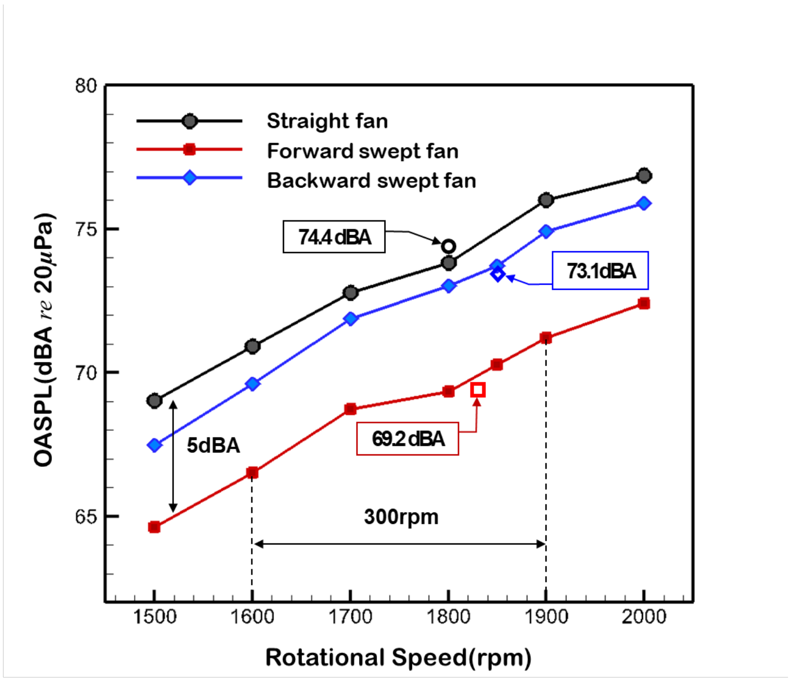

Fig. 5. Overall A-weighted sound pressure levels of the straight, forward- and backward-swept fans depending on rotational speeds (filled symbol: experimental result, open symbol: numerical prediction)

To identify the noise sources and investigate the mechanism for noise reduction in the backward and forward-swept fans, we used the flow field data, including velocity, vorticity, the time derivative of pressure contours, and streamlines. Figs. 6 and 7 show the cross-sectional views of the xz and xy planes of the instantaneous velocity vector around the backward and forward-swept fans, respectively. It can be observed that the flow passing through the forward-swept fan moves toward the centerline of the fan and propagates downstream. However, in the case of the backward-swept fan, the large recirculation flow is observed behind the shroud, thereby preventing the propagation of the flow downstream. In addition, a secondary recirculating flow could lead to the strong blade vortex interaction (BVI) phenomenon near the blade tip region and unsteady flow interaction between the rotating blades and shallow shroud, which are the dominant noise sources in an automotive cooling fan system. Fig. 8 presents the calculated noise contribution mapped on the surface of an automotive cooling fan system to recognize the primary noise source clearly. The noise contribution at the observer is computed by averaging the acoustic data in the time domain for three revolutions. Consequently, a stronger noise source is observed near the leading edge in the tip region of the backward-swept fan than that in the forward-swept fan.

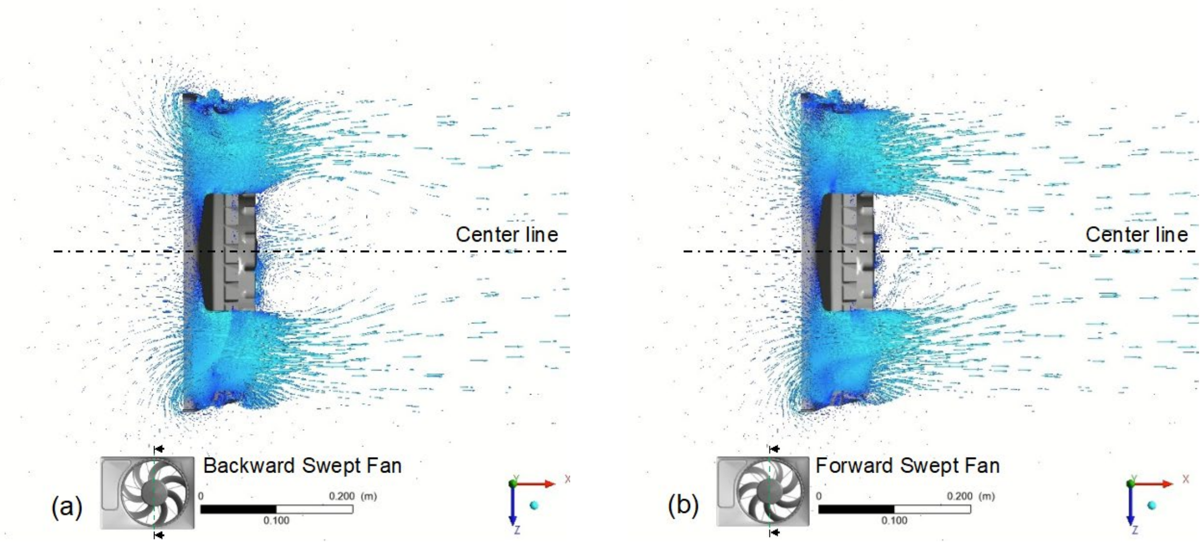

Fig. 6. Velocity vector in the xz plane: (a) backward and (b) forward-swept fans

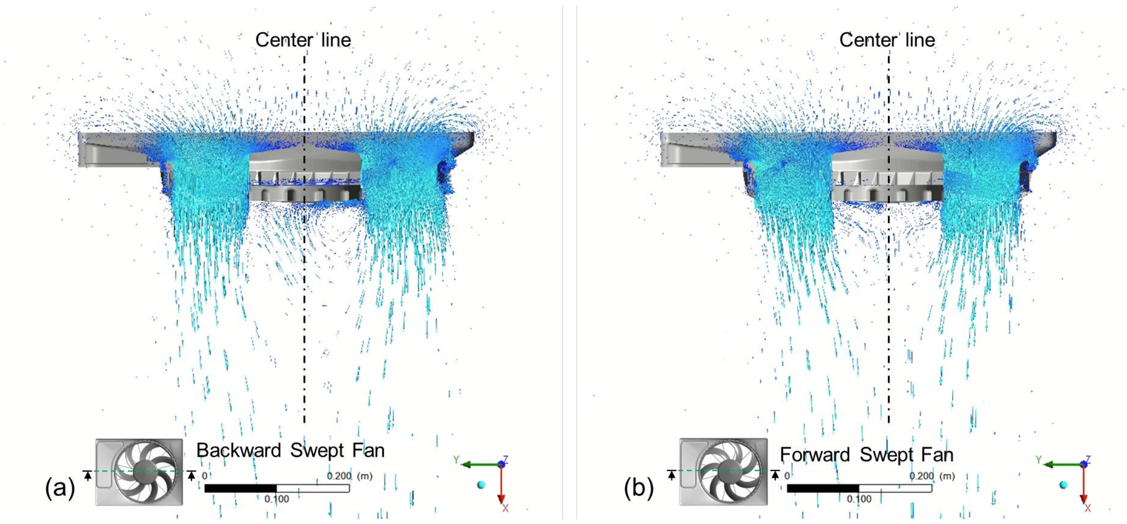

Fig. 7. Velocity vector in the xy plane: (a) backward and (b) forward-swept fans

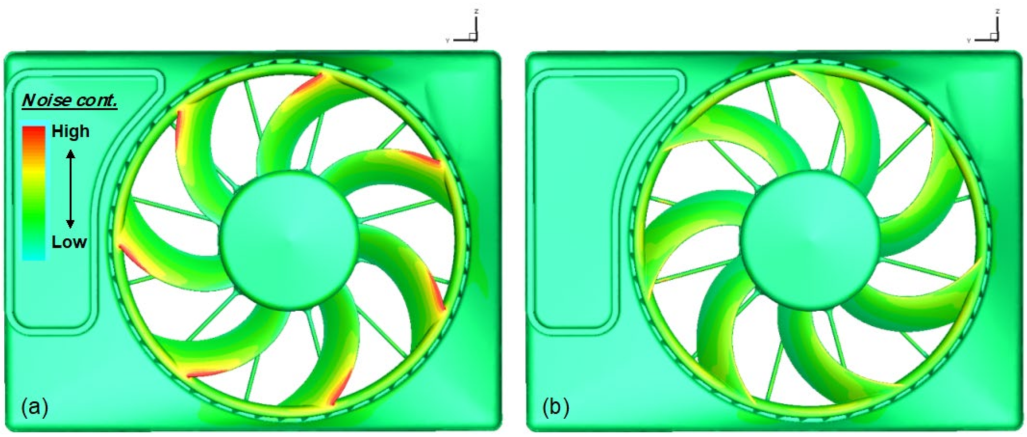

Fig. 8. Averaged noise contributions at the observer: (a) backward and (b) forward-swept fans

Figures 9 and 10 show the contour plots depicting the time derivative of surface pressure on the backward and forward-swept fan on varying the azimuth angles. They are helpful for comparing the magnitude of the noise source and identifying its position because the time derivative of the pressure acting on the surface is one of the noise sources, as in the first term on the right-hand side in Eq. (4). Evidently, the noise source of the backward-swept fan occurs on the leading edge of the mid-span of blades and moves to the blade tip by increasing its intensity, and then it moves towards the trailing edge of the blade between the fan band and the tip. Meanwhile, in the case of the forward-swept fan, the noise source is observed near the leading edge of the blade tip and moves slightly to the hub, and then it also moves toward the trailing edge of the blade between the fan band and the tip. Apparently, the dynamic behaviors of the noise source of the forward-swept fan with varying azimuth angles are different from those of the backward-swept fan. In addition, although the fan system operates under the same condition, the magnitude of the noise source is different depending on the geometrical shape of the swept fan.

Figures 11 and 12 present the instantaneous vorticity contours of the backward and forward-swept fans with varying azimuth angles, respectively, clearly demonstrating the vortex structures on the surface. In the case of the backward-swept fan, little vorticity is generated adjacent to the mid-span of the blade leading edge. Subsequently, the vorticity is increased and the vortex structure moves to the blade tip. After that, it can be observed that the high vorticity is located adjacent to the trailing edge of the blade tip, as shown in Fig. 11 (a). In the case of the forward-swept fan, such as the contour of the pressure-time derivative, it can be observed that high vorticity is generated adjacent to the leading edge of the blade tip. Then the vorticity moves slightly to the hub and goes to the trailing edge.

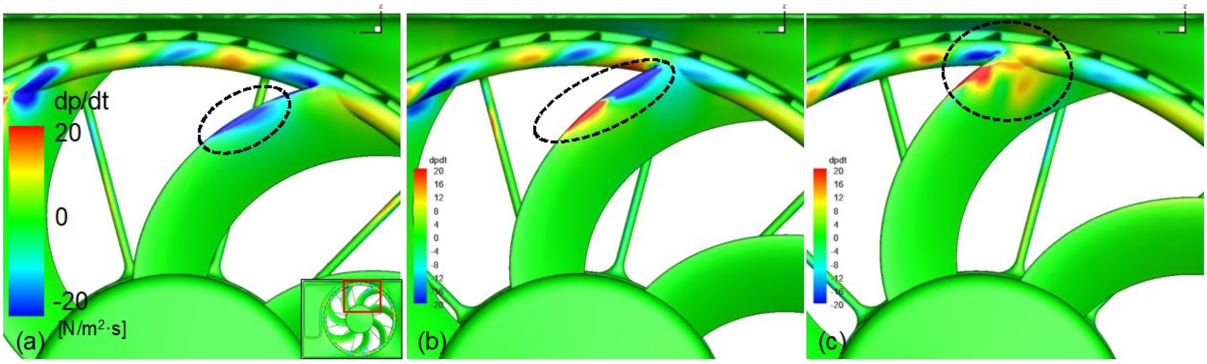

Fig. 9. Time derivative of the surface pressure on backward-swept fan depending on the azimuth angles: (a) 0 degree, (b) 10 degrees, and (c) 20 degrees

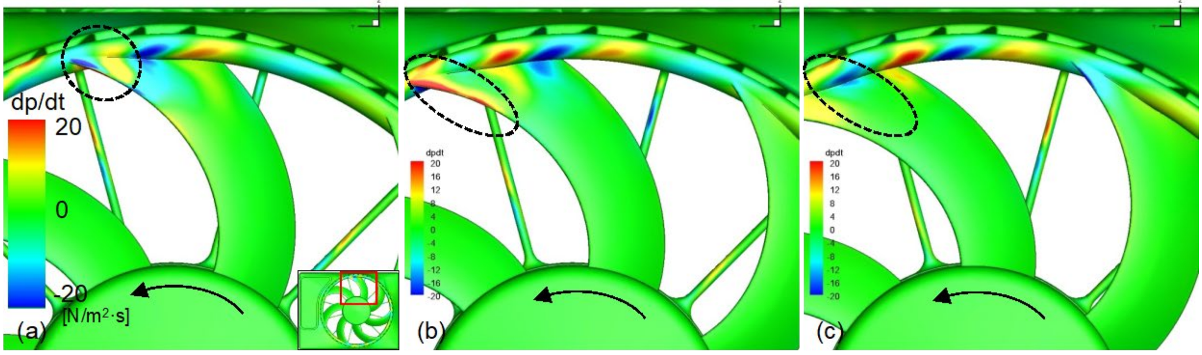

Fig. 10. Time derivative of the surface pressure on forward-swept fan depending on the azimuth angles: (a) 0 degree, (b) 10 degrees, and (c) 20 degrees

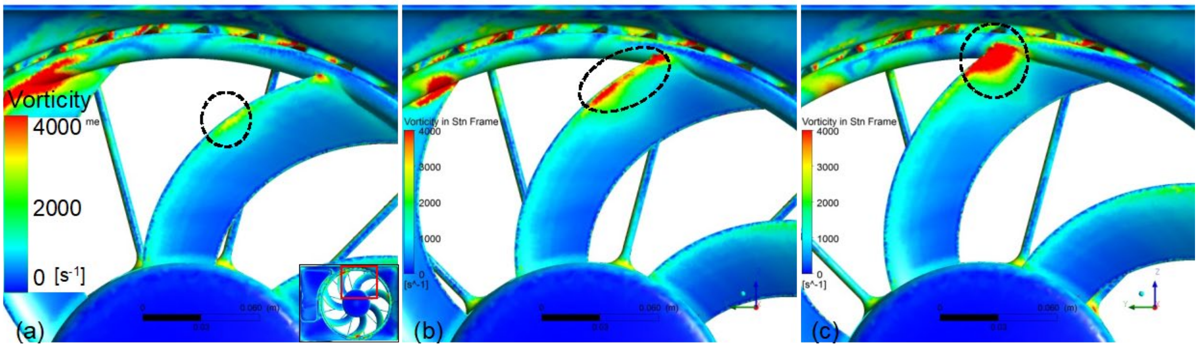

Fig. 11. Vorticity contours of backward-swept fan depending on the azimuth angles: (a) 0 degree, (b) 10 degrees, and (c) 20 degrees

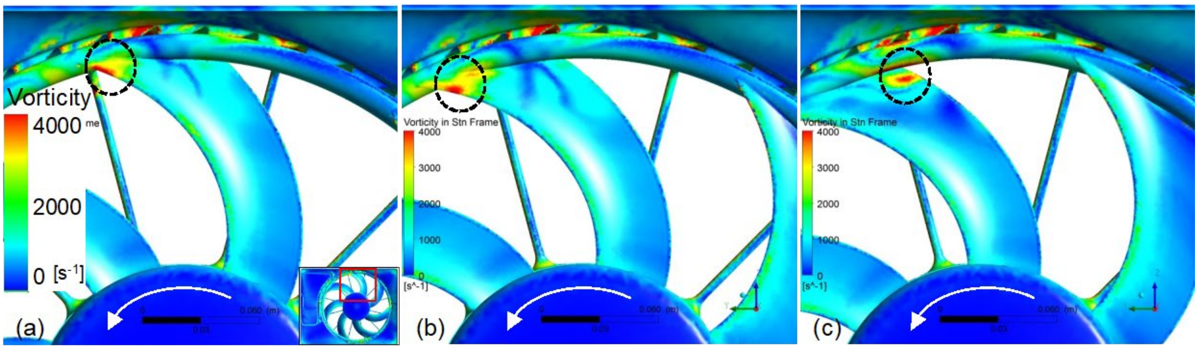

Fig. 12. Vorticity contours of forward-swept fan depending on the azimuth angles: (a) 0 degree, (b) 10 degrees, and (c) 20 degrees

Figure 13 depicts the streamlines on the blade surface of the backward and forward-swept fans. The streamlines of the backward-swept fan move from the leading edge of the blade toward the tip region. Moreover, they traverse a steep slope toward the trailing edge of the tip. Conversely, the streamlines of the forward-swept fan move from the leading edge of the blade toward the hub region, and then they have a smooth slope toward the trailing edge of the hub. The streamline can change depending on the direction of the geometrical blade sweep. In the case of the backward-swept fan, the vortex structures that generated in the leading edge of the mid-span and tip vortex move in the outward radial direction, resulting in a strong interaction between the tip vortex shedding from the blade tip and recirculating flow generated by the shallow section of the serrated shroud. As depicted in Figs. 9 and 11, tip vortex interaction causes unsteady pressure fluctuations, which are the primary noise source in the backward-swept fan. From these observations, the backward-swept blade with accumulated vortices on the blade tip and band has strong interactions with the serrated geometries of the shroud. However, the sweep in the forward direction changes the flow patterns on the blades and helps suppress the tip vortex interaction. In the case of the forward-swept fan, the vortex structures that are generated in the leading edge of the blade tip move in the inward radial direction owing to the geometrically forward-swept shape, thereby alleviating the tip vortex effect interacting with the serrated geometries of the shroud. Therefore, the noise reduction in the forward-swept fan can be achieved by changing the flow direction toward the hub.

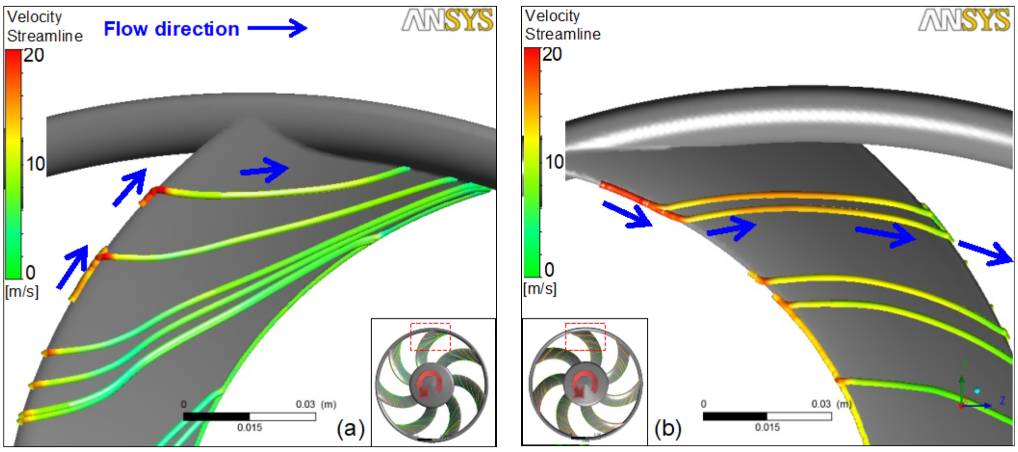

Fig. 13. Instantaneous velocity streamline on the rotor blade: (a) backward and (b) forward-swept fans

4. Conclusion

In this study, we investigated the effects of sweep direction on the noise level and flow physics around an automotive cooling fan, including the serrated shroud. Further, the mass flow rate and sound pressure levels of straight, forward, and backward-swept fans were measured using a standard fan tester and semi-anechoic chamber, respectively. We also calculated them using a hybrid method based on the unsteady RANS simulation and acoustic analogy. Numerical predictions were formulated to identify the dominant noise sources in the cooling fan and to analyze the sweep effects. The experimental results indicated that the forward-swept fan could achieve a higher noise level reduction of 4 dBA than the backward-swept fan and 5 dBA than the straight fan. As evident in the numerical works, the backward-swept fan induced the recirculation flow behind the serrated shroud and accumulated tip vortices near the blade tip and band, leading to the strong flow interaction with the shroud geometry. The BVI phenomenon near the blade tip region caused the pressure fluctuation on the blade surface, which was the dominant noise source in the backward-swept fan. However, by changing the flow pattern in the radial direction of the blade, we observed that the forward-swept blade could help alleviate the tip vortex interaction. Therefore, our findings in the present study provided significant insight into the acoustic characteristics of automotive cooling fans depending on the direction of the swept blade. The results of this study help improve our understanding of the unsteady flow physics of the swept cooling fans with serrated shroud, and they can be used as a guide for designing a low-noise fan blade.

The limitation of this study is that the mass flow rate and sound pressure levels were measured under a zero system resistance condition. Conversely, real automotive cooling fan systems operate under various system resistance levels owing to the existence of other components behind the cooling fan. Thus, in the future, measurements on the performance and noise levels of automotive cooling fans that operate in actual conditions will be conducted using an anechoic fan tester facility, and the effects of the system resistance will further be investigated.

Declaration of competing for interest

The authors declare that they have no known competing financial interests or personal relationships that could have appeared to influence the work reported in this paper.

Acknowledgments

This study was supported by the National Research Foundation of Korea (NRF) grant funded by the Ministry of Science, ICT & Future Planning (NRF-2017-R1A5A1015311, 2020R1I1A1A01066929, and 2021R1C1C1010198)..

References

[1] Longhouse RE. Noise mechanism separation and design considerations for low tip-speed, axial-flow fans. J Sound Vib 1976;48(4):461-474.

[2] Corsini A, Rispoli F, Sheard AG. Development of improved blade tip endplate concepts for low-noise operation in industrial fans. Proceedings of the Institution of Mechanical Engineers, Part A: J Power Energy 2007;221(5):669-681.

[3] Gue F, Cheong C, Kim T. Development of low-noise axial cooling fans in a household refrigerator. J Mech Sci Technol 2011;25(12):2995-3004.

[4] Kim W et al. Development of a low-noise cooling fan for an alternator using numerical and doe methods. Int J Automot Technol 2011;12(2):307-314.

[5] Wang Shuwen et al. Noise reduction of automobile cooling fan based on bio-inspired design. Proc Inst Mech Eng D 2021;235:465-478.

[6] Smith J, Leroy H, Hsuan Y. Sweep and dihedral effects in axial-flow turbomachinery. ASME J Basic Eng 1963;85:401–416.

[7] Denton JD, Xu L. The effects of lean and sweep on transonic fan performance. ASME turbo expo 2002: power for land, sea, and air. Am Soc Mech Eng Dig Collec 2002;23–22.

[8] Cummings RA, Morgan WB, and Boswell RJ. Highly skewed propellers. Transactions of the SNAME 1972;80:98–135.

[9] Fujita H. Noise characteristics and outlet flow field of axial flow fans. NASA STI/Recon Technical Report A1979;79:79–85.

[10] Fukano, T, Kodama Y, Takamatsu Y. Noise generated by low pressure axial flow fans, II: Effects of number of blades, chord length and camber of blade. J Sound Vib 1977;50(1):75–88.

[11] Kerschen E, Envia E. Noise generation by a finite span swept airfoil. 8th Aeroacoustics Conference 1983;768.

[12] Envia E. Fan noise reduction: an overview. Int J Aeroacous 2002;1(1):43–64.

[13] Hanson, Donald B. Influence of propeller design parameters on far-field harmonic noise in forward flight. AIAA J 1980;18(11):1313–1319.

[14] Wright T, Simmons W.E. Blade sweep for low-speed axial fans. J Turbomach 1990;112:151–158.

[15] Carolus T, Beiler M. Skewed blades in low pressure fans: A survey of noise reduction mechanisms. AIAA J 1997;1591:47–53.

[16] Krömer FJ, Moreau, Stefan B. Experimental investigation of the interplay between the sound field and the flow field in skewed low-pressure axial fans. J Sound Vib 2019;442:220–236.

[17] McNulty GS, Decker JJ, Beacher BF, Khalid SA. The impact of forward-swept rotors on tip clearance flows in subsonic axial compressors. J Turbomach 2004;126(4):445–454.

[18] Bamberger K, Carolus K. Optimization of axial fans with highly swept blades with respect to losses and noise reduction. Noise Control Eng J 2012;60(6):716–725.

[19] Hurault J, Kouidri S, Bakir F, Rey R. Experimental and numerical study of the sweep effect on three-dimensional flow downstream of axial flow fans." Flow Measurement and Instrumentation 2010;21(2):155–165.

[20] Zenger F, Herold G, Stefan B. Acoustic characterization of forward-and backward-skewed axial fans under increased inflow turbulence. AIAA J 2017;55(4):1241–1250.

[21] Herold G, Florian Z, Ennes S. Influence of blade skew on axial fan component noise. Int J Aeroacous 2017;16(4–5):418–430.

[22] Gato LMC, Webster M. An experimental investigation into the effect of rotor blade sweep on the performance of the variable-pitch Wells turbine. Proceedings of the Institution of Mechanical Engineers, Part A: J Power Energy 2001;215(5):611–622.

[23] Kim TH, Setoguchi T, Kaneko K, Raghunathan S. Numerical investigation on the effect of blade sweep on the performance of Wells turbine. Renew Energy 2002;25(2):235–248.

[24] Vad J. Aerodynamic effects of blade sweep and skew in low-speed axial flow rotors at the design flow rate: an overview. Proceedings of the Institution of Mechanical Engineers, Part A: J Power Energy 2008;222(1):69–85.

[25] Kingan MJ, Parry AB. Acoustic theory of the many-bladed contra-rotating propeller: analysis of the effects of blade sweep on wake interaction noise. J Fluid Mech 2019;868:385–427.

[26] Ghodake D, Sanjosé M, Moreau S, Henner M. Modification of noise sources by virtue of blade sweep in low speed fan. In: Proceedings of the 26th International Congress on Sound and Vibration, Montreal, QC, Canada. 2019:7–11.

[27] Park M, Lee DJ. Sources of broadband noise of an automotive cooling fan. Appl Acoust 2017;118:66–75.

[28] Wilcox DC. Turbulence Modeling for CFD, Vol. 2. La Canada, CA: DCW industrie 1998.

[29] Longhouse RE. Control of tip-vortex noise of axial flow fans by rotating shrouds. J Sound Vib 1978;58(2):201–214.

[30] Lighthill MJ. On sound generated aerodynamically. I. General theory. Proc R Soc Lond A 1952;211:564–587.

[31] Ffowcs Williams JE, Hawkings DL. Sound generation by turbulence and surfaces in arbitrary motion. Philoso Trans Royal Soc Lond Series A Math Phys Sci 1969;264:321–42.

[32] Neise W. Review of fan noise generation mechanisms and control methods: An International INCE Symposium 1992;45–56

[33] Farassat F, Brentner KS. The acoustic analogy and the prediction of the noise of rotating blades. Theor Comput fluid Dyn 1998;10(1):155–170

[34] Brentner KS. Prediction of helicopter rotor discrete frequency noise for three scale models. J Airc 1988;25(5):420–427.

[35] Lowson MV. The sound field for singularities in motion. Proceedings of the Royal Society of London. Series A. Mathematical and Physical Sciences 1965;286(1407):559–572.

[36] Standard AMCA 210-99. Laboratory Methods of Testing Fans for Aerodynamic Performance Rating, Air Movement and Control Association International Inc 1999;210.